Recognition of Capped RNA Substrates by VP39, the Vaccinia Virus-Encoded mRNA Cap-Specific 2′-*O*-Methyltransferase†

Steve W. Lockless,‡,§ Hui-Teng Cheng,‡ Alec E. Hodel,||,⊥ Florante A. Quiocho,|| and Paul D. Gershon*,‡

Department of Biochemistry and Biophysics, Institute of Biosciences and Technology, Texas A&M University, Houston, Texas 77030, and Howard Hughes Medical Institute and Department of Biochemistry, Baylor College of Medicine, Houston, Texas 77030

Received January 23, 1998; Revised Manuscript Received April 15, 1998

ABSTRACT: We have investigated the interaction of VP39, the vaccinia-encoded mRNA cap-specific 2′-*O*-methyltransferase, with its capped RNA substrate. Two sites on the protein surface, responsible for binding the terminal cap nucleotide (m^7G) and cap-proximal RNA, were characterized, and a third (downstream RNA binding) site was identified. Regarding the crystallographically defined m^7G binding pocket, VP39 showed significant activity with adenine-capped RNA. Although VP39 mutants lacking specific m^7G-contact side chains within the pocket showed reduced catalytic activity, none was transformed into a cap-independent RNA methyltransferase. Moreover, each retained a preference for m^7G and A over unmethylated G as the terminal cap nucleotide, indicating a redundancy of m^7G-contact residues able to confer cap-type specificity. Despite containing the 2′-O-methylation site, m^7GpppG (cap dinucleotide) could not be methylated by VP39, but $m^7GpppGU^{biotin}p$ could. This indicated the minimum-length 2′-*O*-methyltransferase substrate to be either $m^7GpppGp$, $m^7GpppGpN$, or $m^7GpppGpNp$. RNA−protein contacts immediately downstream of the m^7GpppG moiety were found to be pH-sensitive. This was detectable only in the context of a weakened interaction of near-minimum-length substrates with VP39's m^7G binding pocket (through the use of either adenine-capped substrate or a VP39 pocket mutant), as a dramatic elevation of K_M at pH values above 7.5. K_M values for substrates with RNA chain lengths of 2−6 nt were between 160 and 230 nM, but dropped to 9−15 nM upon increasing chain lengths to 20−50 nt. This suggested the binding of regions of the RNA substrate >6 nt from the 5′ terminus to a previously unknown site on the VP39 surface.

VP39 is a bifunctional vaccinia virus protein which participates in the modification of both mRNA ends (*1*−*3*). At the mRNA 5′ end, VP39 specifically methylates the first transcribed nucleotide of the 5′ cap structure, $m^7G(5')pppNp(N)_n$, to its 2′-O-methylated form, $m^7G(5')pppN^mp(N)_n$, in an AdoMet[1]-dependent manner (*4*). At the mRNA 3′ end, VP39 acts as a processivity factor for the vaccinia-encoded poly(A) polymerase, VP55, keeping the polymerase anchored to the nascent oligo(A) tail during elongation of the latter (*1*, *2*, *5*, *6*).

In its 5′ end modifying function, VP39 could be described as a nucleic acid ribose methyltransferase. As such, it does not fall within any class of enzyme whose catalytic mechanism has been well characterized. In a pioneering study of VP39's 2′-*O*-methyltransferase properties, and the only such study to date (*4*), the protein was shown to exhibit specificity for RNAs with the 5′ terminal structure $m^7G(5')pppN$, over GpppG- and pppN-terminated RNAs. However, simple cap-dinucleotides of the form $m^7G(5')pppN$ were very poor substrates for, or inhibitors of, the enzyme. With regard to the sequence of the substrate RNA, VP39 apparently preferred capped poly(A) and poly(I) over other RNA homopolymers, and also exhibited a significant preference for $m^7G(5')pppA$-terminated over $m^7G(5')pppG$-terminated mRNA. The minimum RNA chain length compatible with 2′-*O*-methyl acceptor activity was not reported. VP39 was shown to exhibit Michaelis−Menten kinetics, consistent with a random bireactant mechanism. The genomic RNA of brome mosaic virus (BMV), which comprises four distinct $m^7G(5')pppG$-capped species 876−3234 nt in length (*7*−*9*), was shown to be an efficient substrate, exhibiting a K_M of ∼5 nM (*4*). VP39's pH dependence was also demonstrated, in an experiment showing a bell-shaped 2′-*O*-methyltransferase initial-rate profile with a pH optimum of 7.5. However, it was not shown whether this related to substrate/cofactor binding and/or catalysis. VP39 was shown to interact with its AdoMet cofactor with a K_M of 2 μM, and to be completely inhibited by 1 μM AdoHcy in the presence of 2.5 μM AdoMet. Other experiments showed that 2′-*O*-methyltransferase activity was inhibited by NaCl

† Supported by National Science Foundation Grant MCB-9604188 to P.D.G.

* Correspondence should be addressed to this author at Room 817, IBT, 2121 W. Holcombe Blvd., Houston, TX 77030-3303. Telephone: 713-677-7665. Fax: 713-677-7970. Email: pgershon@ibt03.tamu.edu.

‡ Texas A&M University.

§ Present address: Howard Hughes Medical Institute and Department of Biochemistry, University of Texas Southwestern Medical Center, Dallas, TX 75235.

|| Baylor College of Medicine.

⊥ Present address: Department of Biochemistry, Emory University School of Medicine, Atlanta, GA 30322.

[1] Abbreviations: BMV, brome mosaic virus; AdoMet, *S*-adenosyl-L-methionine; AdoHcy, *S*-adenosyl-L-homocysteine.

S0006-2960(98)00178-0 CCC: $15.00
Published on Web 05/19/1998

at concentrations greater than 50 mM, and that divalent cations are not required for the 2′-*O*-methyltransferase reaction (*4*).

Analysis of VP39's mechanism has been facilitated by the recent solution of a high-resolution cocrystal structure of the protein complexed with (i) its AdoMet cofactor (*10*), (ii) the AdoHcy coproduct plus cap dinucleotide $m^7G(5')pppG$ (*11*), and (iii) AdoHcy plus the capped RNA substrate $m^7G(5')pppG(A)_5$ (*12*). VP39 was shown to be a compact, single-domain protein whose surface forms an oblate sphere. One of the two major faces is bisected with a cleft, one end of which is punctuated with an aromatic-side chain-lined pocket. The pocket interacts with the m^7G moiety of the mRNA cap structure, and the cleft interacts with the three cap-adjacent nucleotides of the capped RNA chain in an apparently sequence-independent manner. The AdoMet cofactor binds a second, shallower pocket perpendicular to the center of the cleft, with its methyl group protruding into the cleft in a position appropriate for catalysis.

In the following study, we investigate properties of the capped RNA substrate suitable for methyl group acceptor activity, define the minimum substrate length, provide evidence for the interaction of VP39 with a downstream RNA segment, and elucidate the effects of pH upon VP39-capped RNA interaction and catalysis.

MATERIALS AND METHODS

Proteins. The m^7G binding pocket mutants used in this study have been described previously (*11*). Mutants Y22A, E233A, and D182A+E233A were made using the 'Chameleon' kit (Stratagene), following the manufacturer's instructions, along with a mutagenesis template encoding N-terminally GST-tagged VP39-ΔC26 [a 26 amino acid C-terminal truncation mutant of VP39 which lacks a portion of the protein's nonfunctional 36−43 residue C-terminal tail (*13, 14*)]. Mutants F180A and D182A were generated as described previously (*13*), using a mutagenesis template identical to that described above except for the presence, between the second and third VP39 codons, of a 21 nt DNA segment encoding the amino acid sequence RRASVEF. The resulting protein, VP39−NΔC26, is indistinguishable from VP39-ΔC26 in its biochemical properties (*15*). Mutant proteins were expressed in *E. coli* as described previously (*11*). All recombinant proteins were purified and cleaved from the GST moiety using thrombin, as described previously, and then subjected to heparin−agarose column chromatography (*10, 16*). All purified proteins were concentrated by ultrafiltration (Amicon Inc.) and their final concentrations determined by a modified version of the Bradford assay (*17*). Final concentrations of proteins were as follows: 0.5 mg/mL or 1.39×10^{-5} M (wild-type VP39-ΔC26), 3.5 mg/mL or 9.7×10^{-5} M (Y22A), 6 mg/mL or 1.67×10^{-4} M (F180A), 5 mg/mL or 1.4×10^{-4} M (D182A), 7 mg/mL or 1.94×10^{-4} M (E233A), and 2 mg/mL or 5.6×10^{-5} M (D182A+E233A), assuming a molecular weight of 36 000 for each protein.

Generation, Quantitation, and Purification of •-$(A)_n$-Based Transcripts. Transcripts of the form •-$(A)_n$, •-$(A)_nU$, and •-$(A)_nU^{biotin}$ were employed here, where •- represents either pppG, GpppG, ApppG, or $m^7G(5')pppG$, or hydrolysis products thereof generated during transcription. $m^7G(5')$-pppG was presumed to be incorporated in either the 'forward' [$m^7G(5')pppG$...] or the 'reverse' [$G(5')pppm^7G$...] orientation during transcription (*18*). All RNAs were generated by in vitro transcription of short, partially double-stranded DNA templates using T7 RNA polymerase (*19*). Template oligonucleotides comprised 5′-CCTAATACGACTCACTAT-AGA-3′ (top strand) along with either 5′- $(T)_n$CTATAGT-GAGTCGTATTAGG-3′ or 5′-A$(T)_n$CTATAGTGAGTCGTA-TTAGG-3′ (bottom strand). Prior to transcription, the two template strands were annealed in TE buffer by heating at 90 °C for 3 min and then cooling on ice. The nucleoside triphosphates/analogues thereof present during transcription comprised ATP, along with either $m^7G(5')pppG$, ApppG, or GTP (for incorporation at the initiating position). For •-$(A)_nU$- and •-$(A)_nU^{biotin}$-based transcripts, either UTP or biotin-21-UTP (Clontech), respectively, was also present. Total volumes of transcription reactions varied from 0.1 to 5 mL. After 3 h incubation at 37 °C, reactions were centrifuged to pellet the Mg-pyrophosphate, and supernatants were stored at −70 °C.

Heterogeneous-length, 2′-O-methylatable transcription products were quantitated by electrophoresis alongside various amounts of oligodeoxynucleotide markers, followed by ultraviolet (UV) shadowing using an imaging plate (*20*). The imaged oligodeoxynucleotide bands were quantitated with background subtraction using a PhosphorImager (Molecular Dynamics Inc.), and the resulting signals were plotted against the known amounts of oligodeoxynucleotide. The portion of each transcription product-containing lane corresponding to RNAs with an apparent length of 4 nt or greater was also quantitated, and RNA amounts (and hence concentrations) were derived from the oligodeoxynucleotide calibration plots. Fifty percent of the quantitated RNA was assumed to be initiated with the cap in the 'forward' orientation, i.e., to be bona fide 2′-O-methylatable substrate.

For the purification of individual RNAs from heterogeneous mixtures of transcription products, supernatants from the Mg-pyrophosphate removal step were injected onto a C18 semipreparative column (Vydac) equilibrated with 0.1 M triethylamine acetate (TEAA) buffer (pH 6.8), using a Milton Roy modular HPLC instrument (comprising two Constametric 3000 pumps, a GM4000 gradient programmer, and a Spectrometric 3100 UV monitor set to 260 nm). The column was eluted at a flow rate of 4 mL/min with linear gradients of acetonitrile in 0.1 M TEAA buffer whose exact profiles varied from one experiment to another. Fractions corresponding to individual peaks were pooled, dried under vacuum, and redissolved in DEPC-treated water. For some individual peaks, the redissolved material was further purified by a second round of C18 column chromatography using a shallower gradient. Again, fractions corresponding to individual peaks were dried under vacuum and redissolved in sterile water. Material purified from the isolated peaks was analyzed by electrospray ionization mass spectrometry (ESI-MS). Concentrations of HPLC-purified short RNAs were determined from OD_{260} values, using molar absorbancy (ϵ_{260}) values of 1.82×10^4 (m^7GpppG), 1.53×10^4 (AMP), and 2.666×10^4 (UMP^{biotin}), giving values of 9.47×10^4 and 2.82×10^4 for $m^7GpppG(A)_5$ and $m^7G(5')pppGpU^{bio}p$, respectively.

For the generation of the short RNA substrate $m^7G(5')$-$pppGpU^{bio}p$, transcription reactions were performed as

described above (in a total volume of 0.25 mL), except that the bottom template strand comprised 5′-$(T)_5$GACTATAGT-GAGTCGTATTAGG-3′, and the sole nucleoside triphosphates/analogues thereof comprised m^7G(5′)pppG, biotin-21-UTP (Clontech), CTP, and [α-^{32}P]ATP. The expected RNA product of this transcription reaction was m^7G(5′)-pppGU^{bio}C$(A)_5$. The Mg-pyrophosphate removal step was followed by the addition of 25 μL of 5 M NaCl and 1 μL of 0.1 mg/mL RNase A. After incubation at 37 °C for 15 min, the sample was subjected to C18 column chromatography as described above (see also the legend to Figure 1E).

2′-O-Methyltransferase Assays. The standard 2′-*O*-methyltransferase assay (*4*) was modified in several respects. Regarding the methylation substrate, the standard BMV RNA was replaced with various in vitro-generated RNA transcripts (above): for assays of 'pocket' mutants (Figure 3), unpurified transcription products from pppG-, GpppG-, ApppG-, and m^7GpppG-initiated transcription reactions (above) were used; for kinetic experiments, C18 column-purified m^7GpppG$(A)_4$ and ApppG$(A)_4$ were employed at the concentrations specified in individual experiments. Reactions at pH 7.5 (or where the pH is not specified) employed the standard 2′-*O*-methyltransferase assay buffer (25 mM HEPES−NaOH, pH 7.5, 1 mM DTT). Assays at other pH values employed the following buffer substances: PIPES−NaOH (pH 6.5); HEPES−NaOH (pH 7.0); Tris-HCl (pH 8.0 and 8.5); and AMPSO (pH 9.0 and 9.5). After adjusting the pH, 0.1 M stock solutions of these buffers were supplemented with 4 mM DTT to provide 4× assay buffers. For each assay, sufficient AdoMet (NET 155H, DuPont NEN) was first dried from the manufacturer's storage buffer for a final concentration of ∼1 μM when redissolved in assay buffer. 2′-*O*-methyltransferase reactions were initiated by the addition of VP39. After various times of incubation at 30 °C, samples were withdrawn and mixed with equal volumes of formamide. Short (6-mer or less) reaction products were then applied to preelectrophoresed 25% polyacrylamide/urea/TBE gels alongside bromophenol blue (BPB) and xylene cyanol markers. 20-mer and 50-mer RNA products were applied to 20% polyacrylamide gels. After electrophoresis, gels were impregnated with fluor (Fluorenhance, RPI) following manufacturer's instructions, and then dried and exposed to preflashed X-ray film. The positions of ^{3}H-methylation products were identified by aligning the film with the original gel (guided by distinguishing marks on the gel), after which the individual [^{3}H]RNA bands were excised from the dried gels and placed in 4 mL of liquid scintillation cocktail (Ultima Gold, Packard). DPM values were obtained using a Packard 2500TR liquid scintillation counter, which compensated for quenching by calculating the transformed spectral index of an external standard. Background DPM values, determined by counting randomly excised regions of the dried gels, were subtracted from other values. Initial 2′-*O*-methylation rates (DPM·s^{-1}), determined from plots of DPM values versus time, were converted to mol·s^{-1} from the known specific activity of the [^{3}H]AdoMet cofactor (3 TBq/mMol, or 180 DPM/fmol). The resulting values were multiplied by 300, a factor introduced to correct for the apparent underestimation of RNA concentration by tritium quantitation after electrophoresis, with respect to spectrophotometric determinations using the ϵ_{260} values given above. This correction factor was derived by exhaustive 2′-O-methylation of spectrophotometrically determined amounts of several small RNAs in the presence of a severalfold molar excess of [^{3}H]AdoMet (which was also present at concentrations greater than VP39's K_M for AdoMet), followed by electrophoresis, band excision, scintillation counting, and conversion of DPM to moles, as described above. Further treatments of the resulting rate data are described in the legends to individual figures.

HPLC-purified m^7G(5′)pppGpU^{bio}p (above) was assayed for methyl-acceptor activity in the standard methyltransferase assay buffer (above). m^7G(5′)pppGpU^{bio}p, [^{3}H]AdoMet (which was not dried from the manufacturer's storage buffer prior to the assay), and crystallographically pure VP39-ΔC26 were present at concentrations of ∼7.3 μM, 0.92 μM, and 0.12 μM, respectively, in a final reaction volume of 60 μL. After incubation for 15 min at 30 °C, 10 μL of streptavidin paramagnetic particle suspension (Dynal Inc.) was separated from the manufacturer's storage buffer and washed once with water (0.5 mL), and then resuspended in 0.5 mL of 1 M NaCl, and the resulting suspension was added to the assay mixture. After an additional 15 min incubation at 30 °C, the beads were collected, washed twice with 0.5 mL of 1 M NaCl and once with 0.5 mL water, and then subjected to scintillation counting as described above.

BIAcore RNA Binding Assay. RNAs of the form •-$(A)_n$-U^{biotin}, for use in BIAcore experiments, were synthesized as described above. BIAcore RNA binding experiments were performed as described previously (*14*). Briefly, streptavidin was covalently immobilized to the sensing surfaces of each of the four flowcells of a BIAcore sensor chip CM5 (BIAcore AB), followed by separate injections of each of the four biotinylated RNA species. Equivalent amounts of each RNA were immobilized within each flowcell by interrupting injections after equivalent increases in signal. For the pH experiments, BIAcore running buffers comprised 20 mM buffer (diluted from the 0.1 M stock solutions described above), plus 0.005% Tween 20 detergent and 60 mM NaCl. Highly purified VP39-ΔC26 (above) was diluted to 0.2 μM in running buffer before injection. After each injection of bound VP39-ΔC26, protein was removed by three sequential injections of 0.5 M NaCl in running buffer. Kinetic rate constants were determined from sensorgrams using the BIAevaluation 2.0 software. Additional experimental details can be found in the legend to Figure 5.

RESULTS

The Minimal RNA Substrate for 2′-O-Methylation by VP39 Is m^7G(5′)pppGp, m^7G(5′)pppGpN, or m^7G(5′)pppGpNp. A recent crystallographic study of the VP39-capped RNA complex (*12*) required the isolation and characterization of various highly purified, short-capped RNAs of the form m^7G-(5′)pppG$(A)_n$. The availability of these RNAs provided an opportunity to characterize the minimum RNA chain length able to support VP39's cap-specific 2′-*O*-methyltransferase activity. RNAs were generated by in vitro transcription of the corresponding partially double-stranded DNA templates in the presence of either GMP, GTP, or m^7GpppG for incorporation as the initiating nucleotide. Transcription of discrete DNA templates directing synthesis of the transcripts G$(A)_5$ and G$(A)_{10}$ led to the production of heterogeneous-length transcripts (Figure 1A, upper panel). Since the

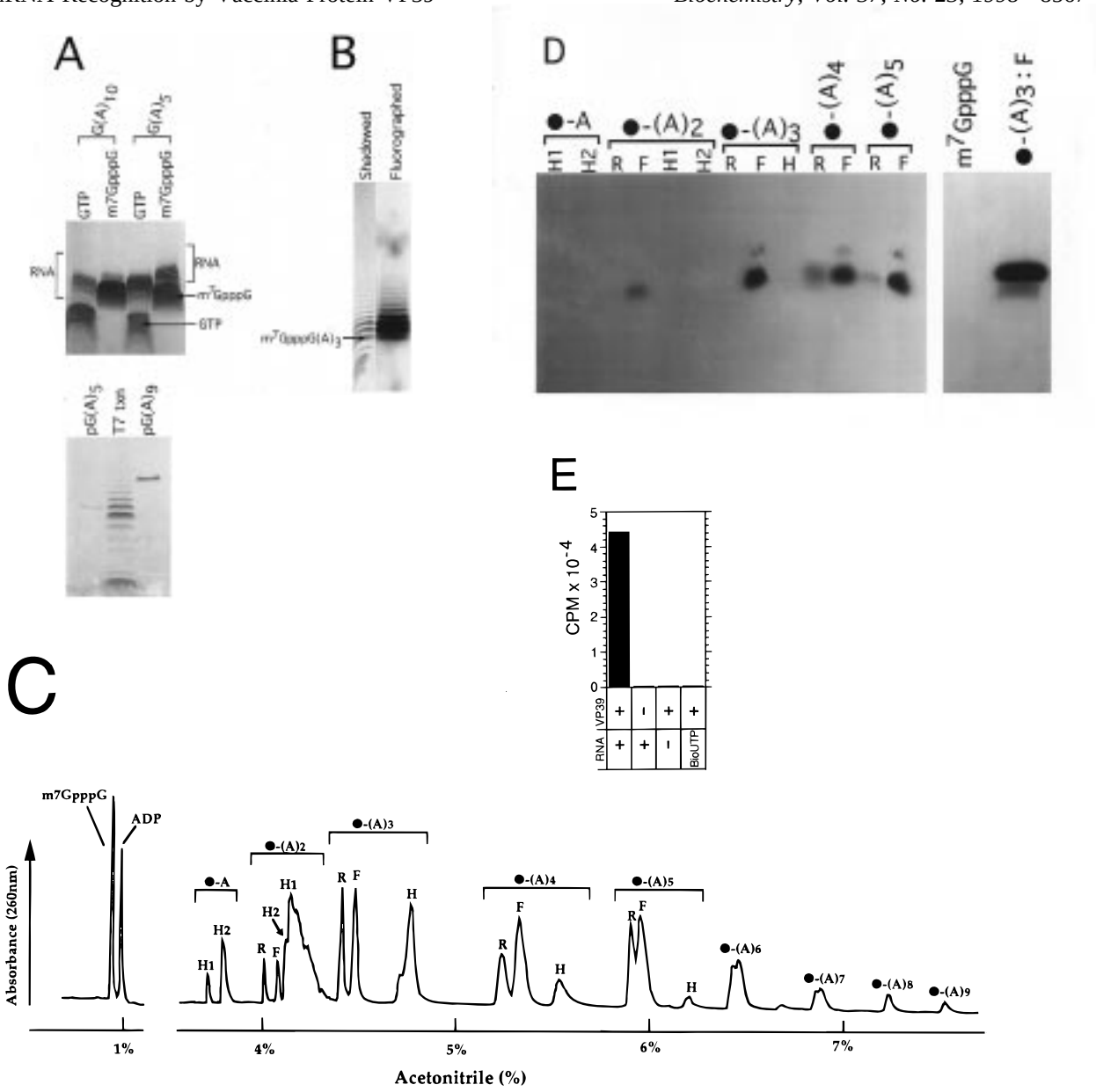

FIGURE 1: Minimum RNA chain length necessary for cap-specific 2′-*O*-methylation. (A) UV-shadowed polyacrylamide gels showing transcription products and size markers. Upper panel: Transcription reactions templating the synthesis of either $G(A)_{10}$ or $G(A)_5$ in which the initiating nucleotide was either GTP or m^7GpppG. Heterogeneous products ('RNA', free nucleotides ('GTP', 'm^7GpppG') are visible. Lower panel: Sizing of transcription products from a $G(A)_5$-templated, GMP-initiated transcription reaction, using 5′-phosphorylated, chemically synthesized $pG(A)_5$ and $pG(A)_9$ RNAs as size markers. (B) In vitro synthesized capped oligo(A) can be 2′-*O*-methylated by VP39. An aliquot of the heterogeneous products of a $G(A)_5$-templated, m^7GpppG-initiated transcription reaction was 2′-*O*-methylated by VP39, and the 2′-*O*-methylated and unmethylated samples were electrophoresed in adjacent lanes of a 25% polyacrylamide gel for UV-shadowing (total RNA) and fluorography (2′-*O*-methylated RNA). The band corresponding to $m^7GpppG(A)_3$ was identified by comparison with gels containing sizing markers (as shown in part A of this figure, lower panel). (C) C18 column chromatogram of $G(A)_5$-templated, m^7GpppG-initiated transcription products. •- denotes multiple 5′ end structures [for example, $m^7GpppG(A)_n$, $Gpppm^7G(A)_n$, $pppG(A)_n$, and $ppG(A)_n$ are denoted •-$(A)_n$]. The gradient comprised 0−9% acetonitrile in 0.1 M aqueous TEAA (pH 6.8), run over a period of 60 min. The resolution of the gradient approached the maximum obtainable with the available instrumentation. See text for further details. (D) Left panel: 2′-*O*-Methylation of material from peaks in part (C), some having been rechromatographed to improve purity. Each RNA was assayed at a concentration of ∼40 μM. Right panel: Attempt to 2′-*O*-methylate commercially prepared cap dinucleotide [m^7G(5′)pppG], at a concentration of 125 μM and over a reaction time of 60 min. As a control, a peak assayed in the left panel was reassayed in parallel. See text for further details. (E) The very short RNA m^7G(5′)pppGpU^{biotin}p was purified by subjecting an RNase A-treated m^7G(5′)-pppGpU^{biotin}C([^{32}P]A)$_5$ transcription reaction to C18 column chromatography (Materials and Methods), eluting with a linear gradient of 0−6% acetonitrile in 0.1 M aqueous TEAA (pH 6.8) over a period of 40 min. Two pairs of significant-sized, nonradioactive peaks eluting late in the chromatogram were considered as candidates for m^7G(5′)pppGpU^{bio}p, the expected nonradioactive RNase A digestion product. Of these, only a single peak (peak 'D') could be 2′-*O*-methylated by VP39 to any significant extent, and was subjected to ESI-MS. The observed molecular mass of 1752 for peak 'D' corresponded well with the theoretical mass of 1752.5 for m^7G(5′)pppGpU^{biotin}p. Peak 'D′ material was incubated with VP39 and [^{3}H]AdoMet, and then recovered from the incubation mixture using streptavidin paramagnetic particles which were subsequently washed and subjected to scintillation counting. See text for additional details.

distribution of transcript lengths was unrelated to template size, the majority of the products were apparently 'abortive' in character. Product arrays initiating with m^7G(5′)pppG electrophoresed with significantly lower mobility than those

initiating with GTP (Figure 1A, upper panel), consistent with the net positive charge associated with the m^{7}G base. To assign sizes to individual transcripts within the product arrays, products from a G(A)$_5$-templated, GMP-initiated reaction were coelectrophoresed with the chemically synthesized RNA markers pG(A)$_5$ and pG(A)$_9$ (Figure 1A, lower panel). This experiment indicated the major transcription product to be pG(A)$_4$, with the larger products decreasing in abundance with size.

To determine whether the short, m^{7}G(5′)pppG(A)$_n$ transcripts could be 2′-*O*-methylated by VP39, an aliquot of the products from an m^{7}G(5′)pppG-initiated, G(A)$_5$-templated transcription reaction was electrophoresed in a 25% polyacrylamide gel alongside a second aliquot which had been incubated with VP39 and [^{3}H]AdoMet under methylation conditions. The gel was UV-shadowed and then fluorographed (Figure 1B). Using Figure 1A (lower panel) to estimate RNA sizes, it appeared that capped oligo(A) RNAs at least as short as 4 transcribed nt [i.e., m^{7}G(5′)pppG(A)$_3$] could be 2′-*O*-methylated. Since the shortest RNAs were not clearly resolved by gel electrophoresis (Figure 1A,B), individual transcription products were systematically isolated by reverse phase (C18) column chromatography. Numerous peaks were obtained upon C18 column chromatography of a set of m^{7}GpppG-initiated G(A)$_5$-templated transcription products identical to those analyzed electrophoretically in Figure 1B (Figure 1C). Using ESI-MS to establish the identity of each peak resolved in the 0−6.3% acetonitrile range, it was concluded that each length of transcript between 3 and 10 transcribed nucleotides contributed a cluster of three peaks to the chromatogram. Within each triple, the peak labeled 'H' (Figure 1C) corresponded in molecular weight to either ppG- or pppG-initiated RNA, and the peaks labeled 'F' and 'R' correspond to m^{7}G(5′)pppG- and G(5′)pppm^{7}G-initiated RNA, respectively. Since peaks F and R have identical molecular mass within each triple, their identities were distinguished by 2′-*O*-methylation. For this experiment, material from each peak in the •-(A)$_3$, •-(A)$_4$, and •-(A)$_5$ triples (where •- denotes the multiple 5′ end structures) was repurified by C18 column chromatography, and the repurified peaks [along with the original peaks for •-A and •-(A)$_2$] were normalized for RNA concentration. Incubation of the resulting RNAs with VP39 and [^{3}H]AdoMet followed by electrophoresis in a denaturing 25% polyacrylamide gel (Figure 1D, left panel) showed that only one of the two m^{7}G(5′)pppG-terminated RNAs within each triple was a bona fide methylation substrate. The substrate and nonsubstrate RNAs were denoted 'F' for 'forward' capped RNA [m^{7}GpppG(A)$_n$] and 'R' for 'reverse' capped RNA [G(5′)pppm^{7}G(A)$_n$], respectively.

Since RNAs as short as m^{7}G(5′)pppG(A)$_2$ were apparently 2′-*O*-methylatable (Figure 1D, left panel), we reexamined the published finding that cap dinucleotide [m^{7}G(5′)pppG] cannot be 2′-*O*-methylated by VP39 (*4*). In our hands, it also could not be detectably 2′-*O*-methylated (Figure 1D, right panel), despite the use of a significantly higher concentration (125 μM) than that employed for the purified chromatographic peaks (~40 μM; Figure 1D, left panel). Thus, the shortest capped RNA substrate for 2′-*O*-methylation by VP39 was apparently either m^{7}G(5′)pppG(N)$_2$ or m^{7}G(5′)pppGN. Since m^{7}G(5′)pppGA was not recovered from m^{7}G(5′)pppG-initiated transcription reactions in detectable quantities due to the overwhelming predominance of 'hydrolysis' peaks H1 (pppGA) and H2 (ppGA) (Figure 1C), an alternative approach was taken to investigate substrates of the form m^{7}G(5′)pppGN. Specifically, the molecule m^{7}G(5′)pppGpU^{biotin}p was generated (see Materials and Methods and legend to Figure 1E). The biotin moiety was included to facilitate magnetic bead-mediated product capture after 2′-*O*-methylation, since this molecule was presumed to be too small for electrophoretic resolution from [^{3}H]AdoMet. When tested for 2′-*O*-methyl acceptor activity at a concentration of ~7.3 μM (Figure 1E), m^{7}G(5′)pppGpU^{biotin}p could clearly be 2′-*O*-methylated (Figure 1E). We conclude that the shortest viable 2′-*O*-methyl acceptor for VP39 is either m^{7}G(5′)pppGp, m^{7}G(5′)pppGpN, or m^{7}G(5′)pppGpNp.

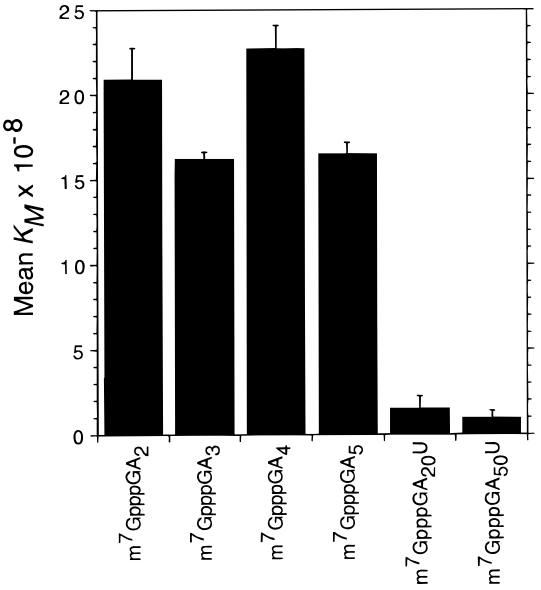

FIGURE 2: Plot showing mean K_M values for various lengths of capped oligo(A). Each RNA was assayed between 2 and 5 times as described in the text, and K_M values were determined separately for each replicate assay. Error bars denote range.

Table 1: Mean K_M Values for Various Lengths of Capped Oligo(A), As Plotted in Figure 2[a]

RNA	mean K_M (M)
m^{7}GpppG(A)$_2$	2.09×10^{-7}
m^{7}GpppG(A)$_3$	1.62×10^{-7}
m^{7}GpppG(A)$_4$	2.27×10^{-7}
m^{7}GpppG(A)$_5$	1.65×10^{-7}
m^{7}GpppG(A)$_{20}$U	1.48×10^{-8}
m^{7}GpppG(A)$_{50}$U	9.30×10^{-9}

[a] For additional details, see text and legend to Figure 2.

Longer RNAs of the Form m^{7}G(5′)pppG(N)$_{>5}$ Are More Active VP39 Substrates. Although very short m^{7}G-capped oligo(A) RNAs could be 2′-*O*-methylated by VP39 (above), it was not clear whether substrate efficacy was influenced by RNA chain length. Therefore, apparent K_M values were determined for m^{7}G(5′)pppG(A)$_2$, m^{7}G(5′)pppG(A)$_3$, m^{7}G(5′)pppG(A)$_4$, m^{7}G(5′)pppG(A)$_5$, m^{7}G(5′)pppG(A)$_{20}$U, and m^{7}G(5′)pppG(A)$_{50}$U (Figure 2, Table 1). Values for m^{7}G(5′)pppG(A)$_{2-5}$ were comparable to one another, in the range (1.6−2.3) × 10^{-7} M. This is ~40 times higher than the value (5 nM) reported previously for BMV RNA (*4*). However, K_M values for two longer RNAs, m^{7}G(5′)pppG(A)$_{20}$U and m^{7}G(5′)pppG(A)$_{50}$U, were ~13- and ~21-fold lower, respectively, than the average for the short capped

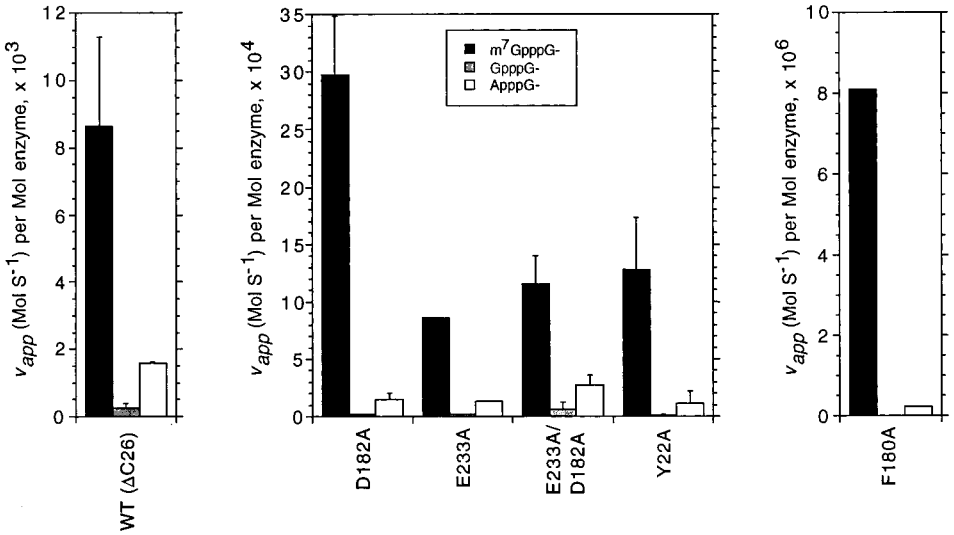

FIGURE 3: Plots showing apparent 2′-*O*-methylation rate (v_{app}) values for heterogeneous •-$(A)_n$ substrates [where •- denotes a 5′ structure comprising either pppG, G(5′)pppG, m^{7}G(5′)pppG or A(5′)pppG] by either wild-type VP39 ['WT (ΔC26)'] or mutants thereof in which residues Y22, F180, D182, E233, or both D182 and E233 are replaced by alanine. Unpurified RNA substrates, prepared as described under Materials and Methods, were diluted 17-fold into the methyltransferase reaction giving final substrate concentrations of ~60 μM. Standard 2′-*O*-methyltransferase assay conditions were used, along with 50 μM S-[*methyl*-^{3}H]adenosyl methionine (80 Ci/mMol, DuPont NEN) and enzyme at the following concentrations: 2.1×10^{-7} M (WT), 1.47×10^{-6} M (Y22A), 2.53×10^{-6} M (F180A), 2.1×10^{-6} M (D182A), 2.94×10^{-6} M (E233A), and 8.5×10^{-7} M (D182A+E233A). For each reaction, 10 μL samples were withdrawn after 1, 3, 9 and 20 min of incubation at 30 °C, transferred to 10 μL of formamide, and subjected to electrophoresis and fluorography. Quantitation was performed by the 'cut and count' method (Materials and Methods). Duplicate assays were performed; error bars denote the range.

RNAs (Figure 2, Table 1). At 9.3 nM, the K_M for m^{7}G(5′)-pppG$(A)_{50}$U was comparable to the value for the much longer BMV RNA (5 nM), determined in the earlier study (*4*). These data indicate that an increase in the length of the m^{7}G-capped RNA chain from 6 to 20 nt enables the RNA substrate to fully occupy the substrate binding sites of VP39, presumably by utilizing a VP39 RNA binding site remote from that for the cap-proximal region of the substrate.

Wild-Type VP39 Can 2′-O-Methylate ApppG-Capped RNA. Having examined characteristics of the substrate RNA chain that promote efficient 2′-*O*-methylation, we explored VP39's specificity for the m^{7}G cap structure. VP39 has been shown to 2′-*O*-methylate m^{7}G(5′)ppp-terminated RNA with a high degree of specificity, with G(5′)ppp- and ppp-terminated RNAs acting as only very poor methyl-group acceptors (*4*). The more recent advent of synthetic cap analogues and purified phage RNA polymerases permits the generation of RNAs initiating with unnatural cap structures. We therefore evaluated RNAs of the form •-$(A)_{3-\sim10}$ as 2′-*O*-methyltransferase substrates, where •- comprises either pppG, G(5′)pppG, m^{7}G(5′)pppG, or A(5′)pppG (Figure 3). As found previously (*4*), uncapped (i.e., 5′-triphosphate-terminated) RNA could not be detectably methylated by wild-type VP39 (data not shown), and G(5′)pppG-terminated RNA exhibited only very low levels of substrate activity [retaining, in our hands, only ~4.6% of the activity of the m^{7}G(5′)-pppG-terminated substrate; Figure 3, left panel]. However, to our surprise, A(5′)pppG-capped substrates could be 2′-*O*-methylated by VP39 to relatively high levels (~20% of those for m^{7}G-terminated RNA; Figure 3, left panel).

Mutation of VP39's Cap Binding Pocket Alters the 2′-O-Methyltransferase Reaction Rate, but Not Substrate Preference. VP39's strong specificity for an N7-methylated terminal cap nucleotide (m^{7}G) over its unmethylated (G) counterpart results from unknown determinants. Cocrystal structures of VP39 with the m^{7}G(5′)pppG cap dinucleotide and with m^{7}G(5′)pp alone (*11*) show the m^{7}G base binding a 'pocket' in VP39's surface, in which the predominant contact residues are D182 (hydrogen bonding to the 2-amino group of m^{7}G), E233 (hydrogen bonding to the N1 imino proton), and Y22 and F180 (stacking with the six-membered portion of the purine ring) (*11*). VP39 did not form cocrystals with guanine-based ligands lacking the 7-methyl group [such as G(5′)pppG and G(5′)pp], consistent with VP39's specificity for m^{7}G(5′)pppG-capped over G(5′)pppG-capped RNA as a 2′-*O*-methyltransferase substrate. However, a strong, direct interaction between VP39 and m^{7}G's 7-methyl group was not apparent. Of a panel of five mutants in which each of VP39's four m^{7}G-contact residues (above) was individually substituted with alanine, one (D182A) appeared to retain full activity in 2′-*O*-methylation and cap-enhanced VP39−RNA interaction; the remaining four (E233A, Y22A, F180A, and D182A+E233A) were impaired (*11*).

We proceeded to determine whether the five m^{7}G-contact residue mutants retained specificity for the m^{7}G cap structure, by assaying them in combination with the four cap-variant substrates described above. Initial rates were determined for each capped RNA/mutant combination (Figure 3). With the m^{7}G(5′)pppG capped RNA substrate, mutants E233A, D182A+E233A, and Y22A each retained ~21−35% of the specific activity of wild-type VP39, while F180A retained only ~0.1% of wild-type specific activity. Like wild-type VP39, none of the mutants showed detectable activity with pppG-terminated (uncapped) RNA (data not shown), indicating that lesions within the m^{7}G binding pocket do not convert VP39 into a cap-independent RNA methyltransferase. Like wild-type VP39, each of the mutants was significantly more active with A(5′)pppG-capped than G(5′)pppG-capped RNA, but less active toward either of these RNAs than the natural m^{7}G(5′)pppG-capped substrate (Figure 3). We conclude that although mutation of m^{7}G-contact residues leads to a

reduction in 2′-*O*-methyltransferase activity, it does not significantly affect substrate specificity.

pH-Dependent VP39−Substrate Interaction and Catalysis. VP39's recognition of the m^{7}G(5′)pppG and A(5′)pppG cap structures in preference to G(5′)pppG (Figure 3) indicated that the exocyclic groups attached to the six-membered portion of the terminal purine ring (i.e., the 2-amino and 6-keto groups of m^{7}G and G, and the 6-amino group of A) might not be critical determinants of m^{7}G cap recognition. Supporting this conclusion is the absence of direct protein contacts with the 6-keto function of m^{7}G in the VP39−m^{7}G(5′)pppG cocrystal structure (*11*), and the minimal loss of 2′-*O*-methyltransferase activity in mutant D182A, which lacks the side chain carboxylate that hydrogen bonds with m^{7}G's 2-amino group (ref. *11*, Figure 3). Assuming no direct role for the 7-methyl group in m^{7}G recognition (above), two factors remain as distinguishing features of m^{7}G: (i) the positive charge delocalized over the five-membered portion of the purine ring; (ii) the pK_a of the N1 imino proton.

To elucidate possible roles for the N1 proton, we examined the effect of pH upon VP39's 2′-*O*-methyltransferase activity over the pH range 6.5−9.5. For these experiments, substrates comprised purified versions of the short RNAs m^{7}G(5′)pppG(A)$_4$ and A(5′)pppG(A)$_4$. First, profiles of pH vs apparent initial 2′-*O*-methylation rate (v_{app}) were determined for the two substrates at various concentrations (Figure 4A,B). The bell-shaped profiles for m^{7}G(5′)pppG(A)$_4$ (Figure 4A) were comparable to the curve reported previously using the longer, equivalently capped BMV RNA (*4*) except that, in our hands, v_{app} peaked at pH ∼8.0 instead of pH 7.5. For the A(5′)pppG(A)$_4$ substrate, maximum v_{app} values were ∼20-fold lower than those for m^{7}G(5′)pppG(A)$_4$ (Figure 4B), and the pH value corresponding to the peak initial rate was found to shift progressively upward with substrate concentration (Figure 4B). Data with the A(5′)pppG(A)$_4$ substrate could not be obtained above pH 8.5, due to the occurrence of extremely low methylation rates. Since VP39 obeys Michaelis−Menten kinetics (*4*), the data from Figure 4A,B could be transformed into Lineweaver−Burk format for further analysis. Figure 4C shows apparent K_M values for the two substrates over the pH range 6.5−9.5. For m^{7}G(5′)pppG(A)$_4$, K_M remained constant with pH at a value comparable to that given in Table 1. For A(5′)pppG(A)$_4$, K_M values remained constant over the pH range 6.5−7.5 at levels ∼6-fold higher than those for m^{7}G(5′)pppG(A)$_4$, but rose steeply at pH values above 7.5 (rising ∼25-fold between pH 7.5 and 8.5). This rise in K_M with pH for A(5′)pppG(A)$_4$ accounts for the observation, in Figure 4B, of a substrate concentration-dependent increase in the optimal pH. This is because, at pH 8.0 and 8.5, the K_M is greater than the lowest two substrate concentrations assayed, and therefore has a negative impact on reaction rates. VP39's catalytic activity with the A(5′)pppG(A)$_4$ substrate would therefore be reflected most accurately by the pH profile observed at the highest substrate concentration. The undetectably low reaction rates for A(5′)pppG(A)$_4$ at pH values above 8.5 presumably reflect a continuing rise in K_M.

We approach the data up to this point in terms of a four-site model in which VP39 possesses (i) an m^{7}G binding pocket which can also interact with the cap-terminal adenine of ApppG-capped RNA, (ii) a catalytic center, (iii) a downstream RNA binding site ('downstream site 1') which interacts with the second and possibly third transcribed nucleotides of the RNA and/or associated phosphates, and (iv) a far-downstream RNA binding site ('downstream site 2') which interacts with regions of the RNA somewhere beyond the sixth transcribed nucleotide. A(5′)pppG(A)$_4$ might be one of the simplest of all possible model substrates, since: (a) it is too short to interact with downstream site 2, (b) its cap-terminal adenine is uncharged, and possesses no ligands for D182 and E233, the two ionizable side chains in VP39's m^{7}G binding pocket which interact directly with m^{7}G (above), and (c) no part of its structure (including the cap-terminal adenine) would be expected to show significant changes in ionization state over the pH range tested. Considering these factors, the only plausible explanation for the rise in K_M for A(5′)pppG(A)$_4$ with pH (Figure 4C) might be a loss of affinity resulting from amino acid side chain deprotonation(s) at downstream site 1. In contrast to A(5′)pppG(A)$_4$, m^{7}G(5′)pppG(A)$_4$ showed no dramatic changes in K_M with pH. Assuming both substrates utilize the same binding site(s), m^{7}G(5′)pppG(A)$_4$ can presumably overcome a loss of affinity at downstream site 1 through its higher affinity for the m^{7}G binding pocket. We reasoned that if the rise in K_M with pH observed upon combining the adenine-capped substrate with wild-type VP39 was due to a weakened interaction at the m^{7}G binding pocket, then it might be recapitulated upon combining m^{7}G-capped RNA with a pocket mutant. The pH vs K_M profile was therefore determined for the m^{7}G(5′)pppG(A)$_4$ substrate in combination with m^{7}G pocket mutants Y22A and E233A (Figure 4D). As predicted, the K_M rose sharply above a critical pH value (in this case, pH 9.0), contrasting with the pH profile of wild-type VP39 with the identical substrate (Figure 4C), and confirming that the interaction can be weakened via the protein as well as the RNA. Since the K_M rise was shifted from pH >7.5 (A-capped RNA, Figure 3C) to pH >9.0 (pocket mutants, Figure 3D), the side chain mutations are presumably better tolerated than the A-cap in the pH range 7.5−9.0. We conclude that the pH-dependent rise in K_M is not a property of the adenine cap per se, but results from pH dependence at downstream site 1 in combination with a weakening of the interaction of the terminal cap residue with the m^{7}G binding pocket.

Finally, k_{cat} values were derived for the m^{7}G(5′)pppG(A)$_4$ and A(5′)pppG(A)$_4$ substrates (Figure 4E,F). The extremely low k_{cat} values for both substrates at all pH values suggest exceptionally low turnover rates. Peak k_{cat} values with A(5′)pppG(A)$_4$ were ∼33-fold lower than with m^{7}G(5′)pppG(A)$_4$. k_{cat} values for m^{7}G(5′)pppG(A)$_4$ exhibited a bell-shaped pH profile between pH 6.5 and 9.5, centered on pH 8.0. With A(5′)pppG(A)$_4$, k_{cat} values were also observed to rise between pH 6.5 and 8.0, and then either remain constant or drop slightly between pH 8.0 and 8.5.

m^{7}G-Dependent Enhancement of the RNA−VP39 Interaction Is pH-Dependent. Since the pH dependence of VP39's 2′-*O*-methyltransferase kinetic parameters appeared to result, at least in part, from VP39's interaction with the RNA chain (above), direct evidence was sought for pH sensitivity in the VP39−RNA interaction. BIAcore methodology provides an accurate, real-time means of investigating the association and dissociation characteristics of pairs of interacting biomolecules, and has previously been used to analyze VP39−RNA interactions (*14*). It was therefore used here. Four RNAs

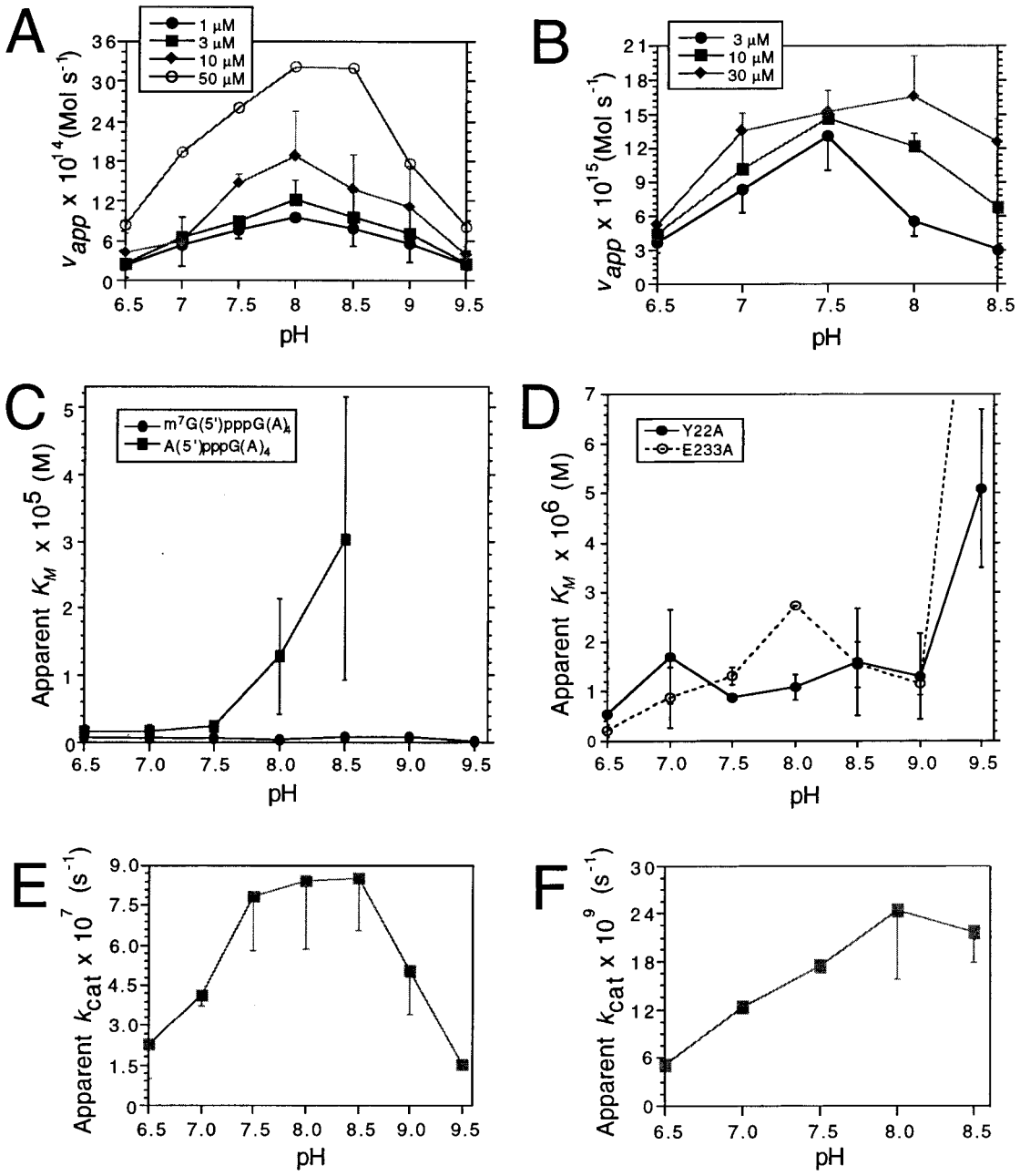

FIGURE 4: Effect of pH on VP39's 2′-*O*-methyltransferase kinetics with two C18 column-purified substrates, m^7G(5′)pppG(A)$_4$ and A(5′)pppG(A)$_4$. Since forward- and reverse-capped m^7G(5′)pppG(A)$_4$ were not well resolved during purification, preparations of this substrate contained ~50% forward- and ~50% reverse-capped RNA, and the concentrations given below refer only to the forward-capped component. (A) pH vs apparent initial rate(v_{app}) profiles for the substrate m^7G(5′)pppG(A)$_4$ at four concentrations: 1 μM (●), 3 μM (■), 10 μM (◆), and 50 μM (○). Initial rates were calculated from the linear initial portions of plots of time vs amount of product formed. The single assay shown with 50 μM substrate employed an $[E]_0$ (VP39 concentration) of 0.3 μM. Assays with 1, 3, and 10 μM substrate were performed in duplicate with individual $[E]_0$ values of 0.3 and 0.7 μM. Mean values are shown for the latter assays, with error bars denoting the range. For simplicity, only a single error bar is shown for each data point (extending either above or below the data point). (B) pH vs v_{app} profiles for the substrate A(5′)pppG(A)$_4$ at three concentrations: 3 μM (●), 10 μM (■), and 30 μM (◆). $[E]_0 = 1$ μM; other details are as for part (A). (C) pH vs apparent K_M profiles for substrates m^7G(5′)pppG(A)$_4$ (●) and A(5′)pppG(A)$_4$ (■). For each of the two substrates at each pH, data from panels A and B were transformed into Lineweaver−Burk format, and, after linear regression, K_M was taken as $-1/x$-intercept. Mean values from duplicate experiments are shown; error bars denote the range. Despite the fairly large differences between absolute K_M values calculated from the individual experiments for A(5′)pppG(A)$_4$, the same sharp rise in K_M between pH 7.5 and 8.5 was observed within each individual experiment. (D) pH vs apparent K_M profiles for substrate m^7G(5′)pppG(A)$_4$ in combination with m^7G binding pocket mutants Y22A (●) and E233A (○). Other details are as described for panel (C). (E) k_{cat} values for substrate m^7G(5′)pppG(A)$_4$. k_{cat} values were calculated for each data point in panel A, using K_M values from the same experiment (panel C) and the Michaelis−Menten transformation $[k_{cat} = v_{app}(K_M + [S])/[E]_0[S]]$. Mean k_{cat} values were then calculated, with error bars denoting the range. For simplicity, only a single error bar is shown for each data point. (F) k_{cat} values for substrate A(5′)pppG(A)$_4$. Values were derived as described for panel E, using the data shown in panels B and C. Other details are as described for panel D.

of the form •-$(A)_{50}U^{biotin}$ (where •- represents pppG, GpppG, ApppG, or m^7GpppG) were immobilized via their 3′-biotin moieties in separate flowcells of a BIAcore sensor chip, and assayed for interaction with injected VP39 at a series of pH values between 6.5 and 9.5. Figure 5A shows the levels of VP39-ΔC26 that became bound to each of the four RNAs

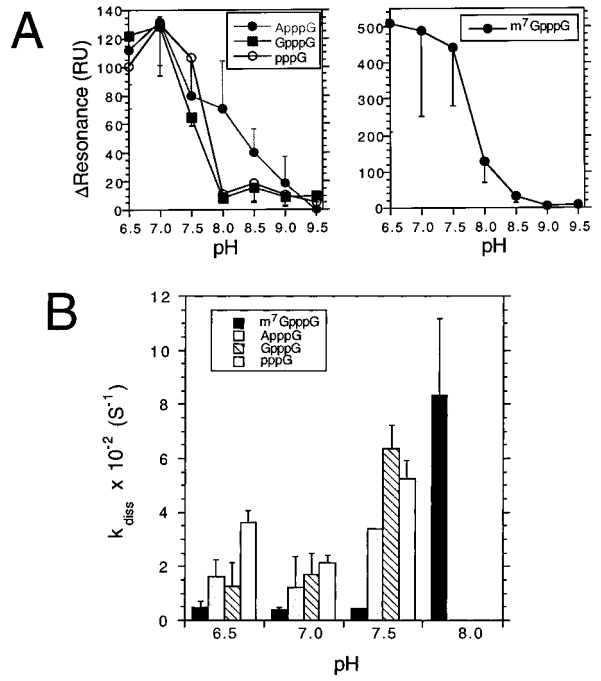

FIGURE 5: pH dependence of VP39−RNA interactions in the BIAcore RNA binding assay. (A) Levels of VP39 bound (RU) at equilibrium, to the four RNAs $pppG(A)_{50}U^{biotin}$, $GpppG(A)_{50}U^{biotin}$, $ApppG(A)_{50}U^{biotin}$, and $m^7GpppG(A)_{50}U^{biotin}$. The four RNAs (∼750 RU of each) were immobilized via their 3′-biotin moieties in separate flowcells of a BIAcore biosensor chip; then VP39-ΔC26 (0.2 μM) was injected to each. The ordinate ('ΔResonance') shows the difference between signals at the start and end of VP39 injection. Each assay was conducted in duplicate. Mean values are shown; error bars denote the range. For simplicity, only a single error bar is shown for each data point. (B) Apparent k_{diss} values derived from 13 of the 28 sensorgrams contributing data to panel A, by exponential curve fitting to the sensorgrams' dissociation phases. Mean k_{diss} values are shown; error bars denote the range. At pH values greater than 8.0 (m^7G-capped RNA) or 7.5 (the other three RNAs), low binding levels prohibited determination of k_{diss}.

at equilibrium. At all pH values at which significant RNA binding was detected, ∼5-fold greater amounts of VP39 became bound to the immobilized m^7G-capped RNA at equilibrium than to the ppp-, Gppp-, and Appp-terminated RNAs (Figure 5A), consistent with previous observations of m^7G cap-enhanced RNA binding in the BIAcore, at pH 8.0 (*11*, *14*). Each of the four RNAs showed sigmoidal profiles of pH vs bound protein, with the greatest binding at low pH and a steep drop in apparent affinity between pH 7.5 and 8.0. Since the VP39−RNA interaction appears to be pH-dependent irrespective of the 5′ cap structure or absence thereof, these profiles strongly indicated that the pH-sensitive interaction occurs at an RNA chain binding site rather than VP39's m^7G binding pocket. Although the identity of this RNA chain binding site is unknown, its properties are consistent with those expected of 'downstream site 1'.

Apparent k_{diss} (dissociation rate constant) values were derived from 13 of the 28 sensorgrams contributing data to Figure 5A, by exponential curve fitting to the sensorgrams' dissociation phases. In the pH range 6.5−7.5, apparent k_{diss} values for VP39's interaction with m^7G-capped RNA were significantly lower than those for the other three RNAs (Figure 5B), indicating that the m^7G-cap significantly retards RNA dissociation from the enzyme. At pH 8.0, the dissociation rate constant for m^7G-capped RNA rose dramatically, and values could not be determined for the other three RNAs due to the very low levels of overall binding observed. Above pH 8.0, binding levels for all of the RNAs were too low for apparent k_{diss} determination. These k_{diss} values (Figure 5B) would contribute to the higher steady-state binding levels observed with m^7G-capped RNA than with the other three RNAs (Figure 5A). It is unclear whether faster association also contributes. Although apparent k_{ass} values for the m^7G-capped RNA remained relatively constant between pH 6.5 and 7.5 (at between 5×10^4 and 10^5 M^{-1} s^{-1}, data not shown), it was not possible to determine meaningful apparent k_{ass} values outside of this pH range or for the other three RNAs, due to the difficulty in obtaining precise apparent k_{diss} values (see error bars in Figure 5B), which are required for k_{ass} curve fitting. The apparent k_{ass} and k_{diss} values for m^7G-capped A_{50} RNA−VP39 interaction in the pH range 6.5−7.5 (above) suggest an apparent K_d of 5×10^{-8} to 10^{-7}.

DISCUSSION

2′-O-Methyltransferase Activity and RNA Chain Length. The VP39 2′-*O*-methyltransferase is specific for m^7G-capped RNA. Although the m^7G cap structure and the RNA chain moiety are both essential components of the substrate, chain moieties as short as two or three transcribed nucleotides are sufficient for substrates to become 2′-*O*-methylated (Figure 1). Substrates with RNA chain lengths of 3−6 nt each exhibited comparable K_M values (Figure 2, Table 1), indicating that nucleotides 4−6 of the RNA chain do not have an important role in substrate anchoring. This finding is reflected in the cocrystal structure of VP39 with $m^7GpppG(A)_5$ (*12*), in which only nucleotides 1−3 of the RNA chain interact with the region immediately adjacent to the 2′-*O*-methyltransferase catalytic center (VP39's 'cleft'). To our surprise, K_M values for substrates with longer RNA chains [$m^7GpppG(A)_{20}U$ and $m^7GpppG(A)_{50}U$] were ∼13−∼21-fold lower than for the short substrates described above. Other data (not shown) indicated that the lower K_M values for the longer substrates resulted from the increased RNA chain length rather than their possession of a 3′-terminal uridylate. Although it is not clear whether there is a precise chain length associated with the transition to a lower K_M, the drop can presumably be attributed to a second RNA binding site distinct from VP39's cleft (denoted 'downstream site 2', above). Since there is little space on VP39's cleft face for the binding of RNA beyond the m^7G cap moiety and first three nucleotides of the RNA chain (*12*), downstream site 2 would presumably be associated with a different part of the protein. Interestingly, the VP39−$m^7GpppG(A)_5$ cocrystal structure showed not only the m^7G moiety and first three nucleotides of the RNA chain interacting with VP39's 'cleft' face, but also the 3′-terminal adenine of the RNA binding an 'adenine-binding pocket' on the 'reverse' face of a symmetry-related VP39 molecule (*12*). It is not clear whether the adenine binding pocket could comprise all or part of downstream site 2. If it does, then a substrate molecule would need to simultaneously bind both the cleft and adenine binding pocket of a single VP39 molecule for the lower K_M value to be observed, as opposed to bridging two distinct protein molecules, the arrangement in the VP39−$m^7GpppG(A)_5$ cocrystal. $m^7GpppG(A)_5$ may be too short to do this (as indicated by molecular modeling; A. Hodel,

data not shown), leading to this substrate's high K_M (Figure 2, Table 1) as well as its arrangement within the crystal. If downstream site 2 coincides with the adenine binding pocket, a preference of VP39 for adenine-containing 2′-*O*-methyltransferase substrates might be expected. This would result not only from the adenine-specific geometry of the adenine binding pocket but also from the apparently sequence-nonspecific RNA binding properties of VP39's cleft/downstream site 1 (*12*). Although an earlier study (*4*) indicated capped poly(A) to be a significantly more active 2′-*O*-methyltransferase substrate than capped poly(G), poly(C), or poly(U), capped poly(I) was also a highly active substrate. Modeling studies indicate that the adenine binding pocket would bind inosine only poorly (A. Hodel, data not shown), leaving the substrate efficacy of capped poly(I) unaccounted for unless the pocket were either distinct from or comprised only a part of downstream site 2.

Factors in VP39's Recognition of Adenine and m⁷G. The experiment of Figure 3 indicates the following ranking of cap structures in terms of their apparent affinity for VP39: m⁷GpppG > ApppG > GpppG. Since this ranking was unchanged in any one of a comprehensive panel of mutants in which each of VP39's four crystallographically defined m⁷G-contact side chains (Y22, F180, D182, E233) was individually ablated (Figure 3), it can be concluded that, assuming specificity does not result from some interaction distinct from these four side chains, there is redundancy among them in the conferrence of cap-type specificity. One pair of side chains within this group likely to have redundant (overlapping) functions might be those of the Y22−F180 m⁷G-stacking sandwich (*11*): Either one of these two aromatic side chains alone might be capable of conferring specificity for m⁷G, by interacting with its partially delocalized positive charge.

It is unclear what features of the terminal adenine of the A-cap permit its recognition in preference to the terminal guanine of the G-cap, despite the m⁷G-cap and G-cap being more closely related to one another than either one is to the A-cap. The only feature of the purine ring m⁷G shares with adenine but not guanine would be an unprotonated N1 nitrogen at pH values between ∼7.5 and ∼9.2 (the pK_a values of N1 imino groups of m⁷G and G, respectively). However, an unprotonated N1 nitrogen would seem unlikely to be important for m⁷G recognition since, in the BIAcore studies (Figure 5), elevation of pH to values above 7.5 appears to destabilize rather than stabilize VP39's interaction with m⁷G-capped RNA. Furthermore, the hypothetical recognition of an unprotonated N1 would imply the absence of a hydrogen bond observed in the VP39−m7Gpp cocrystal, namely, that between the N1 proton and the side chain carboxylate of residue E233 (*11*). This would presumably weaken rather than strengthen the cap−protein interaction. Perhaps the recognition of adenine somehow results from some unique feature, such as adenine's 6-amino group.

Effects of pH on 2′-O-Methyltransferase Substrate−VP39 Interaction. The K_M for a short A-capped RNA substrate rose with pH above 7.5, but for the equivalent m⁷G-capped substrate it did not (Figure 4C). Since protonic transitions could be expected in neither the terminal adenine of the A-cap nor contact side chains in the m⁷G binding pocket over the pH range tested (pH 6.5−8.5), the steep rise in K_M with pH cannot easily be explained by a protonic transition in the interaction of the m⁷G binding pocket with the noncognate adenine cap. Instead, the critical factor might be the relative weakness of the pocket's interaction with the adenine cap. Support for this comes from the observation of a comparable pH-dependent rise in K_M upon weakening the pocket−cap interaction from the protein side (i.e., combining m⁷G capped RNA with VP39 mutants containing substitutions in VP39's m⁷G-binding pocket, Figure 4D). Above (Results), we introduced a model in which VP39 interacts with its capped RNA substrate via four sites on the protein surface, namely, the m⁷G binding pocket, the methyltransferase catalytic center, 'downstream RNA binding site 1', and 'downstream RNA binding site 2'. Since the RNA substrates used in pH studies were too short to interact with downstream site 2, this would leave downstream site 1 (the binding site for a segment of RNA chain immediately adjacent to the 5′ cap structure) as the strongest candidate for a protonic transition that can affect the K_M. Thus, the pH-dependent rise in K_M for adenine-capped RNA would result from a weakened interaction at the m⁷G binding pocket in combination with a protonic transition at downstream site 1. The BIAcore data showing that the decrease in VP39−RNA affinity with increasing pH above 7.5 is independent of the 5′-terminal structure (Figure 5) reflect the apparent pH profile of downstream site 1. However, since the BIAcore experiments measure only VP39's overall RNA binding activity as opposed to its affinity for 2′-*O*-methyltransferase substrate, and also employed much longer RNA ligands than those used in the activity assays, BIAcore signals cannot be assigned with certainty to individual RNA binding site(s) of VP39.

Effects of pH on 2′-O-Methyltransferase Chemical Steps. m⁷G- and A-capped RNAs showed qualitatively similar k_{cat} vs pH profiles (Figure 4E,F). It is not clear whether they are identical, due to difficulties obtaining accurate k_{cat} values for A-capped RNA above pH 8.5 (due to the very low 2′-*O*-methylation rates resulting from the pH-dependent increases in K_M). The k_{cat} vs pH profiles presumably relate directly to the chemical steps of methyl group transfer (though pH-dependent AdoMet binding cannot be ruled out). Both m⁷G- and A-capped RNA substrates exhibit similar (4-fold) increases in k_{cat} between pH 6.5 and 8.0, consistent with this ascending arm of the profile being independent of m⁷G-specific protonic transitions. The ascending arm presumably results from the loss of a proton from an acidic group. If k_{cat} is only related to the chemical steps, then the negatively charged form of the acidic group would promote catalysis. One candidate for this acidic group would be the target ribose 2′OH of the substrate, whose deprotonation might be favored with increasing pH in the 6.5−8.0 range within the protein microenvironment. The descending arm of the k_{cat} vs pH profile (i.e., above pH 8.0−8.5) would result from the loss of a proton from a more basic group. The simplest model for 2′-*O*-methyltransferase activity requires a positively charged group to stabilize the developing negative charge on the attacking O^- of the ribose during a simple bimolecular methyl group transfer reaction. Due to its proximity to the 2′-*O*-methyltransferase catalytic center (*12*), the basic side chain of residue K175 may play this role. The descending arm may, alternatively, result from the pH sensitivity of downstream site 1, affecting substrate anchoring close to the catalytic center.

ACKNOWLEDGMENT

We thank Guanghui Hu for the expression and purification of VP39 mutants E233A and Y22A. This paper is dedicated to the memory of Sergei N. Khilko, who taught one of us (P.D.G.) so much about the BIAcore, kinetics, and the Ukranian perspective.

REFERENCES

1. Gershon, P. D., Ahn, B.-Y., Garfield, M., and Moss, B. (1991) *Cell 66*, 1269−1278.
2. Gershon, P. D., and Moss, B. (1993) *J. Biol. Chem. 268*, 2203−2210.
3. Schnierle, B. S., Gershon, P. D., and Moss, B. (1992) *Proc. Natl. Acad. Sci. U.S.A. 89*, 2897−2901.
4. Barbosa, E., and Moss, B. (1978) *J. Biol. Chem. 253*, 7698−7702.
5. Moss, B., Rosenblum, E. N., and Gershowitz, A. (1975) *J. Biol. Chem. 250*, 4722−4729.
6. Nevins, J. R., and Joklik, W. K. (1977) *J. Biol. Chem. 252*, 6939−6947.
7. Ahlquist, P., Dasgupta, R., and Kaesberg, P. (1984) *J. Mol. Biol. 172*, 369−383.
8. Dasgupta, R., and Kaesberg, P. (1982) *Nucleic Acids Res. 10*, 703−713.
9. Ahlquist, P., Luckow, V., and Kaesberg, P. (1981) *J. Mol. Biol. 153*, 23−38.
10. Hodel, A. E., Gershon, P. D., Shi, X., and Quiocho, F. A. (1996) *Cell 85*, 247−256.
11. Hodel, A. E., Gershon, P. D., Shi, X., Wang, S.-M., and Quiocho, F. A. (1997) *Nat. Struct. Biol. 4*, 350−354.
12. Hodel, A. E., Gershon, P. D., and Quiocho, F. A. (1998) *Mol. Cell 1*, 443−447.
13. Schnierle, B. S., Gershon, P. D., and Moss, B. (1994) *J. Biol. Chem. 269*, 20700−20706.
14. Shi, X., Yau, P., Jose, T., and Gershon, P. D. (1996) *RNA 2*, 88−101.
15. Shi, X., Bernhardt, T. G., Wang, S.-M., and Gershon, P. D. (1997) *J. Biol. Chem. 272*, 23292−23302.
16. Gershon, P. D., and Moss, B. (1996) in *Methods in Enzymology* (Kuo, L. C., Olsen, D. B., and Carroll, S. S., Eds.) pp 208−227, Academic Press, Inc., Orlando.
17. Bradford, M. M. (1976) *Anal. Biochem. 72*, 248−254.
18. Pasquinelli, A. E., Dahlberg, J. E., and Lund, E. (1995) *RNA 1*, 957−967.
19. Milligan, J. F., and Uhlenbeck, O. C. (1989) *Methods Enzymol. 180*, 51−62.
20. Hendry, P., and Hannan, G. (1996) *BioTechniques 20*, 258−264.

BI980178M